Multiply scattered lidar return from water-droplet clouds

V.V. Bryukhanova,* I.V. Samokhvalov,*
A.I. Abramochkin, S.A. Abramochkin, and A.A. Tikhomirov

Tomsk State University
Institute of Optical Monitoring,
Siberian Branch of the Russian Academy of Sciences, Tomsk

The lidar equation obtained earlier for the inhomogeneous atmosphere with regard for single and double scattering is under analysis. It is shown that double scattered forward—backward and backward—backward photon trajectories equally contribute to the backscattering signal intensity. This significantly simplifies the lidar equation providing the sounding pulse penetrates into the cloud to the depth that is small as compared to the scattering volume diameter at the cloud top. It is shown that the double scattered lidar return is more sensitive to aerosol microstructure than the single scattered one. A lidar with a changeable field of view is described allowing one to separate the multiple scattering component in the total lidar return. The technique for estimating the multiply scattered lidar return is based on the hypothesis about normal distribution of multiply scattering intensity in the image plane of the scattering volume at a given distance. The results of experimental investigation of the structure of the lidar return multiply scattered by a droplet cloud are discussed.

Introduction

High sensitivity of lidars at detection of minor aerosol admixtures in the atmosphere, long range, and short time needed to get the data favor their use in studying the dynamics of evolution and spread of cloud formations, as well as temporal transformation of microphysical aerosol characteristics.

Nowadays the data of lidar experiments are interpreted using the lidar equation (LE) obtained with regard for single scattering:

$$P^{(1)}(r) = \frac{P_0 A c \tau_p}{8\pi r^2} X(\pi, r)\sigma(r)e^{-2\tau(r)}, \qquad (1)$$

where $P^{(1)}(r)$ is the power of the single scattered backward radiation coming to the lidar receiving system from the distance r; P_0 is the peak power of the pulse sent to the atmosphere; A is the area of the lidar receiving aperture; c is the speed of light in air; τ_p is the laser pulse duration; $X(\pi, r)$ is the scattering phase function in the direction of 180° with respect to the sensing radiation; $\sigma(r)$ is the volume scattering coefficient at the distance r; $\tau(r) = \int\limits_0^r \alpha(z)\mathrm{d}z$ is the optical thickness at the path segment from 0 to r; $\alpha(z)$ is the volume extinction coefficient determined by the scattering $\sigma(z)$ and absorption $\kappa(z)$ coefficients:

$$\alpha(z) = \sigma(z) + \kappa(z).$$

At sensing atmospheric aerosols, the wavelength λ is selected in the spectral interval free of strong absorption lines of atmospheric gases. In this case, we can assume $\alpha(z) \approx \sigma(z)$.

Radiation propagation in dense scattering media is accompanied by multiple scattering (MS). MS is more sensitive to variations of the sensed medium microstructure as compared to single scattering and, thus, preferable for solution of the inverse problem.[1–6] In the case of sensing clouds, fogs, and dense hazes, the laser radiation is scattered many times before it comes to the lidar receiver, therefore it is necessary to take into consideration in the lidar signal the energy fluxes of all scattering multiplicities reaching the lidar receiving system:

$$P(r) = P^{(1)}(r) + P^{(2)}(r) + \ldots + P^{(i)}(r). \qquad (2)$$

The MS phenomena in aerosol media is properly described by the radiative transfer equation (RTE), which is not yet generally solved. The Monte Carlo method and small-angle approximation are most widely used as approximate methods for the RTE solution. These methods give rather good results in solution of the direct problem, that is, when calculating backscattered signals. At the same time, it is difficult to interpret the data of laser sensing of aerosols, because it is impossible to analyze how the spatial structure of the backscattered signal and the intensities of different scattering multiplicities are connected with lidar parameters and optical characteristics of the medium.

Investigation of regularities of lidar return formation through numerical RTE solution by the Monte Carlo method shows that the first and the second multiplicity scattering mainly contributes to the reflected signal at laser sensing of dense aerosol formations with $\tau \leq 3$ (Ref. 7). The technical capabilities of relatively simple modern lidars allow receiving return signals from the distances not exceeding the optical thickness $\tau \approx 4$. Thus, in many practically important cases the lidar signal can be described in the double scattering approximation with sufficient accuracy, and, based on this, the

inverse problem of aerosol microstructure determination can be solved.[6] Below we consider in detail how a double scattered lidar return is formed in a medium to demonstrate, in the first turn, that the obtained equations for $P^{(2)}(r)$ are no less rigorous than the LE in the form (1).

1. Double scattered lidar return

Consider how a flux of double scattered radiation is formed on the input aperture A of the receiving system of a monostatic lidar (Fig. 1).

The radiation from the source positioned at the point O is directed along the axis Z of the sensing path. The directional pattern of radiation emitted by the source is determined by the linear angle $2\theta_p$, and that of the field of view is determined by $2\theta_0$; and $\theta_p < \theta_0 \ll 1$. Assume that the optical axes of the transmitting and receiving antennae coincide, which is characteristic of monostatic coaxial lidars. The laser pulse can be represented as $P_0(t) = P_0 f(t)$, where $f(t)$ is the function describing the pulse shape.

Let the source at the time $t_0 = 0$ emit a pulse along the axis Z. Then for any $t > 0$ the signal reflected by the medium from the distance $r = ct/2$ can be represented as a sum of single and multiply scattered fluxes. The double scattered flux $P^{(2)}(r)$ is a sum of elementary fluxes $dP^{(2)}$, which arise at successive interaction of radiation with pairs of elementary medium volumes dV_1 and dV_2. The volume dV_1 is located on the axis of the sensing beam at the point O_1, while dV_2 is located at the point $M(z)$ ($0 \leq z \leq r$) lying on the arc RN of an ellipse with the focal points O and $O_1(z)$.

To find the entire return signal caused by the double scattered radiation, we have to sum up $dP^{(2)}$ all over the volume of the scattering medium bounded by a conical surface with the vertex angle $2\theta_0$ and the sphere of the radius $OR = r$ (the cone vertex and the center of the sphere are at the point O). It should be also taken into account that at the time $t = 2r/c$ the double scattered radiation comes to the receiver only from those pairs of dV_1 and dV_2, whose coordinates meet the equation

$$l_1 + l + z = 2r, \tag{3}$$

where l_1 is the distance from the point O to the volume dV_2, l is the separation between the volumes dV_1 and dV_2.

At the fixed position of the point O and the given sensing range r, Eq. (3) is true, if the points $M(z)$, R, and N are on the surface of an ellipsoid of rotation around the axis OZ with the focuses at the points O and $O_1(z)$. The ellipsoid crossing by the plane passing through the axis OZ gives the ellipse equation, having the following form in the polar coordinates:

$$l = r(r - z) / \left(r - z \sin^2 \frac{\gamma}{2} \right), \tag{4}$$

where γ is the polar angle measured in the counterclockwise direction from the positive direction of the axis OZ.

Write the equation for the elementary double scattered signal $dP^{(2)}$ caused by scattering, first, at the point O_1 lying on the axis of the sensing beam and then at the point $M(z)$ belonging to the ellipsoid surface. It has the following form:

$$dP^{(2)}(r) = \frac{A}{16\pi^2} P_0 f\left(t - \frac{2r}{c}\right) \sigma(z) X(z, \gamma) T(z) T(l) \times$$

$$\times \frac{1}{l^2 l_1^2} T(l_1) \sigma(l) X(l, \pi - \gamma) dz dV_2, \tag{5}$$

where

$$T(z, l, l_1) = T(z)T(l)T(l_1) = \exp\{-[\tau(z) + \tau(l) + \tau(l_1)]\}$$

is the medium transmittance on the path;

$$OO_1 + O_1M + MO = 2r,$$

and $\tau(z, l, l_1)$ is the optical thickness at the corresponding path segments. Since $\theta_0 \ll 1$, it can be believed that the extinction α and scattering σ coefficients, as well as the scattering phase function $X(\gamma)$ depend only on the coordinate z. Then in Eq. (5) we can set

$$T(z, l, l_1) \approx \exp\left[-2\int_0^r \alpha(z)dz\right] = \exp[-2\tau(z)].$$

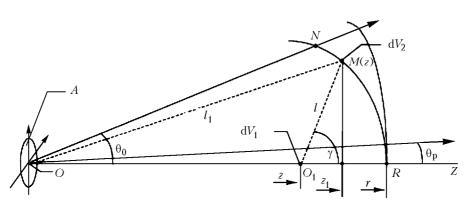**Fig. 1.** Formation of the double scattered flux.

To find the total power of the double scattered radiation $P^{(2)}(r)$ coming to the lidar receiving system for the time from t to $t + \tau_\mathrm{p}$ (simultaneously with the single scattered radiation), we should integrate Eq. (5) all over the volume V_z for any z and then calculate the integral over z. It should be taken into account that V_z depends on the position of the point O_1 on the axis $Z,$ that is, the lower limit of integration over z. The volume V_z is formed by the conical surface with the vertex angle $2\theta_0$ and two ellipsoids of rotation (around OO_1) with the radius vectors l' and l meeting the equations

$$l + l_1 + z = 2r, \quad l' + l_1' + z = 2(r - \Delta r),$$

where $\quad \Delta r = \dfrac{1}{2}c\tau_\mathrm{p}$.

Substituting the equation for $\mathrm{d}V_2 = = l^2\sin\gamma\mathrm{d}\gamma\mathrm{d}\psi\mathrm{d}l$ into Eq. (5) and taking into account that

$$\mathrm{d}l = \frac{l_1^2}{r^2 - (2r - z)z\sin^2(\gamma/2)}\mathrm{d}r, \text{ and } \mathrm{d}r = \frac{c\mathrm{d}t}{2},$$

we integrate Eq. (5) over the azimuth angle ψ from 0 to 2π and then over time from t to $t + \tau_\mathrm{p}$. In the case of sensing by a short pulse $\tau_\mathrm{p} \ll 2/c\varepsilon_{max}$ (ε_{max} is the maximum value of the extinction coefficient on the path under study), the time integral can be easily calculated for $r \gg c\tau_\mathrm{p}$. The power of the double scattered lidar return has the form

$$P^{(2)}(r) = \frac{P_0 A c \tau_\mathrm{p}}{16\pi}e^{-2\tau(r)} \times$$

$$\times \left[\int_0^{\theta_0}\int_0^r \frac{\sigma(z)\sigma(z_1)X(z,\gamma)X(z_1,\pi-\gamma)\sin\gamma}{r^2 - (2r - z)z\sin^2\left(\dfrac{\gamma}{2}\right)}\mathrm{d}z\mathrm{d}\gamma + \right.$$

$$\left. + \int_{\theta_0}^{\pi}\int_{z^*(\gamma)}^r \frac{\sigma(z)\sigma(z_1)X(z,\gamma)X(z_1,\pi-\gamma)\sin\gamma}{r^2 - (2r - z)z\sin^2\left(\dfrac{\gamma}{2}\right)}\mathrm{d}z\mathrm{d}\gamma \right]. \quad (6)$$

Here

$$z^*(\gamma) = r\left(1 - \tan\frac{\theta_0}{2}\cot\frac{\gamma}{2}\right),$$

$$z_1 = z + l\cos\gamma = z + \frac{r(r - z)\cos(\gamma)}{r - z\sin^2\left(\dfrac{\gamma}{2}\right)}.$$

Equation (6) for the lower limit of integration over z was obtained from the condition that at the point N the ellipse (4) intersects the straight line ON, whose equation in the polar coordinate system (pole at the point z) has the form

$$l_1(\gamma) = z\sin\theta_0 \,/[\sin(\gamma - \theta_0)].$$

Equation (6) determines the double scattered lidar return from an arbitrarily stratified medium. It was derived practically within the framework of assumptions on the medium properties and lidar

parameters that are commonly used at formulation of RTE (1) in the single scattering approximation.

When sensing clouds separated from the lidar by the distance H, scattering and extinction of optical radiation in a cloud $\sigma(H \leq z \leq r)$ are usually large as compared to that in the undercloud haze layer at the sensing path segment $0 \leq z \leq H$. Therefore, we can assume $\sigma(0 \leq z \leq H) \approx 0$. In this case, the general equation for $P^{(2)}(r)$ has the form[8]:

$$P^{(2)}(r) = \frac{P_0 A c \tau_\mathrm{p}}{16\pi}e^{-2\tau(r)}[I_1 + I_2], \quad (7)$$

where

$$I_1 = \int_{\theta_0}^{\pi/2}\int_H^r \frac{\sigma(z)\sigma(z_1)}{R(z,\gamma,r)}X(z,\gamma)X(z_1,\pi-\gamma)\sin\gamma\mathrm{d}\gamma\mathrm{d}z,$$

$$I_2 = \int_{\pi/2}^{\pi}\int_{z_{H(\gamma)}}^r \frac{\sigma(z)\sigma(z_1)}{R(z,\gamma,r)}X(z,\gamma)X(z_1,\pi-\gamma)\sin\gamma\,\mathrm{d}\gamma\,\mathrm{d}z;$$

$$R(z,\gamma,r) = r^2\cos^2\frac{\gamma}{2}\left(1 + \frac{(r - z)^2}{r^2}\tan^2\frac{\gamma}{2}\right);$$

$$z_1 = z + \frac{r(r - z)\cos\gamma}{r - z\sin^2\dfrac{\gamma}{2}}, \quad z_{H(\gamma)} \approx r\left(1 - \frac{r - H}{r}\cot^2\frac{\gamma}{2}\right).$$

It can be seen from Eq. (7) that the double scattered lidar return is formed in the cloud medium and depends on both the field of view of the lidar receiving antenna and on the depth of the pulse penetration into the cloud.

2. Peculiarities of formation of double scattered lidar return from remote cloud formations

In dense aerosol media (for example, natural low-level and middle-level clouds), the lidar signal power decreases fast as the laser radiation propagates deeper into the medium. When sensing such media, the depth of pulse penetration into a cloud is small as compared to the distance H to the closest boundary of an aerosol formation:

$$\frac{r - H}{r} \approx \frac{r - H}{H} \ll 1. \quad (8)$$

In this case, it is necessary to take into account that the scattering volume is bounded on the lidar side by a plane, which is determined by the cloud bottom boundary in the case of ground-based sensing and by the cloud top boundary in the case of airborne or spaceborne sensing. If the condition (8) is fulfilled and

$$r - H \leq H\tan\frac{\theta_0}{2}, \quad (9)$$

then Eq. (7) can be significantly simplified.[9]

First of all, it should be noted that if

$$H \le z \le r \text{ and } \frac{r-z}{r} \ll 1,$$

then in Eq. (7)

$$z_1 \approx r\left(1 - \frac{r-z}{r}\tan^2\frac{\gamma}{2}\right).$$

Now we substitute in Eq. (7)

$$\xi = (r-z)\bigg/\left(H\tan\frac{\theta_0}{2}\right),$$

and then in the equation for $I_2(\xi, \gamma)$ change the variables

$$U = \xi\tan^2\frac{\gamma}{2}; \ \beta = \pi - \gamma.$$

After these substitutions, the integrals in Eq. (7) for $I_1(\xi, \gamma)$ and $I_2(U, \beta)$ turn out to be identical. Therefore, Eq. (7) can be rewritten as

$$P^{(2)}(r) = \frac{P_0 A c \tau_p H}{4\pi r^2}\tan\frac{\theta_0}{2}e^{-2\tau(r)} \times$$

$$\times \int_0^{\pi/2}\int_0^{\xi_0}\sigma(\xi)\sigma(\xi_1)X(\xi,\gamma)X(\xi_1,\pi-\gamma)\tan\frac{\gamma}{2}\mathrm{d}\xi\mathrm{d}\gamma.$$

Here it is taken into account that

$$0 \le \xi \le 1, \ \xi_1 = \xi\tan^2\frac{\gamma}{2} \text{ and } \xi_0 = (r-H)\bigg/\left(H\tan\frac{\theta_0}{2}\right).$$

The contribution of the double scattering relative to single one is determined as

$$\delta_{21}(r) = \frac{P^{(2)}(r)}{P^{(1)}(r)} = \frac{2H}{X(\pi,r)\sigma(r)}\tan\frac{\theta_0}{2} \times$$

$$\times \int_0^{\pi/2}\int_0^{\xi_0}\sigma(\xi)\sigma(\xi_1)X(\xi,\gamma)X(\xi_1,\pi-\gamma)\tan\frac{\gamma}{2}\mathrm{d}\xi\mathrm{d}\gamma.$$

Optical characteristics of a homogeneous cloud can be presented as

$$\sigma(z) = \begin{cases} 0, & X(z,\gamma) = 0, & 0 \le z \le H, \\ \sigma_0, & X(z,\gamma) = X(\gamma), & z \ge H. \end{cases} \quad (10)$$

Taking this into account, we obtain the following equations for the power $P^{(2)}(r)$ and relative contribution of double scattering as compared to single one $\delta_{21}(r)$:

$$P^{(2)}(r) = \frac{P_0 A c \tau_p \sigma_0^2 (r-H)}{4\pi r^2}e^{-2\tau(r)}\int_0^{\pi/2}X(\gamma)X(\pi-\gamma)\tan\frac{\gamma}{2}\mathrm{d}\gamma$$

$$(11)$$

and

$$\delta_{21}(r) = \frac{2\sigma_0(r-H)}{X(\pi)}\int_0^{\pi/2}X(\gamma)X(\pi-\gamma)\tan\frac{\gamma}{2}\mathrm{d}\gamma .$$

If the cloud layer is bounded by the heights H and H_1 and the following condition is fulfilled:

$$r - H_1 \le r\tan\frac{\theta_0}{2},$$

then at $r > H_1$ the power of the single scattered signal is $P^{(1)}(r) = 0$, and that of the double scattered signal is

$$P^{(2)}(r) = \frac{P_0 A c \tau_p H}{4\pi r^2}\tan\frac{\theta_0}{2}e^{-2\tau(r)} \times$$

$$\times \int_{\gamma_1}^{\pi/2}\int_{\xi_2}^{\xi_0^1}\sigma(\xi)\sigma(\xi_1)X(\gamma)X(\pi-\gamma)\tan\frac{\gamma}{2}\mathrm{d}\xi\mathrm{d}\gamma,$$

where

$$\xi_0^1 = \frac{r-H}{H\tan\dfrac{\theta_0}{2}}, \ \xi_2 = \frac{r-H_1}{H\tan\dfrac{\theta_0}{2}};$$

$$\gamma_1 = 2\arctan\sqrt{1 - \frac{H_1-H}{r-H}}.$$

For a homogeneous layer ($\sigma = \text{const}$), the following equation is valid:

$$P^{(2)}(r) = \frac{P_0 A c \tau_p \sigma_0^2 (H_1-H)}{4\pi r^2}e^{-2\tau(\Delta H)} \times$$

$$\times \int_{\gamma_1}^{\pi/2}X(\gamma)X(\pi-\gamma)\tan\frac{\gamma}{2}\mathrm{d}\gamma, \quad (12)$$

where $\Delta H = H_1 - H$ is the thickness of the cloud layer.

It follows from Eq. (12) that the double scattered signal comes to the lidar receiver even at the moments $t > 2H_1/c$, when the single scattered signal is zero ($r > H_1$). Thus, the elongation of the lidar signal is explained by the multiple scattering (in this case, double scattering), and the signal tail is determined by the shape of the scattering phase function and the layer thickness.

If $r - H > H\tan\dfrac{\theta_0}{2}$, then the cross size of the scattering volume for the second scattering multiplicity is determined by both the medium boundary and the field of view of the lidar receiving system.

In this case, the general equation for the power of the lidar signal caused by double scattering has the form

$$P^{(2)}(r) = \frac{P_0 A c \tau_p}{16\pi}e^{-2\tau(r)}[I_1 + I_2 + I_3], \quad (13)$$

where

$$I_1 = \int_0^{\gamma_1}\int_H^r\frac{\sigma(z)\sigma(z_1)}{R(z,\gamma,r)}X(z,\gamma)X(z_1,\pi-\gamma)\sin\gamma\,\mathrm{d}\gamma\mathrm{d}z ,$$

$$I_2 = \int\limits_{\gamma_1}^{\gamma_2} \int\limits_{z^*(\gamma)}^{r} \frac{\sigma(z)\,\sigma(z_1)}{R(z,\gamma,r)} X(z,\gamma) X(z_1,\pi-\gamma)\sin\gamma\,\mathrm{d}\gamma\,\mathrm{d}z \,,$$

$$I_3 = \int\limits_{\gamma_2}^{\pi} \int\limits_{z_{H(\gamma)}}^{r} \frac{\sigma(z)\,\sigma(z_1)}{R(z,\gamma,r)} X(z,\gamma) X(z_1,\pi-\gamma)\sin\gamma\,\mathrm{d}\gamma\,\mathrm{d}z \,.$$

Here

$$\gamma_1 = 2\arctan\!\left(\frac{r}{r-H}\tan\frac{\theta_0}{2}\right),$$

$$\gamma_2 = \pi - 2\arctan\!\left(\frac{H}{r-H}\tan\frac{\theta_0}{2}\right).$$

Through the corresponding substitution we can show that Eq. (13) can be reduced to the form

$$P^{(2)}(r) = \frac{P_0 A c \tau_{\mathrm{p}} H}{4\pi r^2}\tan\frac{\theta_0}{2}e^{-2\tau(r)} \times$$

$$\times\left\{\int\limits_0^{\gamma_1}\int\limits_0^{\xi_0}\frac{\sigma(\xi)\sigma(\xi_1)X(\xi,\gamma)X(\xi_1,\pi-\gamma)}{1+\xi^2\dfrac{H^2}{r^2}\tan^2\dfrac{\gamma}{2}\tan^2\dfrac{\theta_0}{2}}\tan\frac{\gamma}{2}\mathrm{d}\xi\,\mathrm{d}\gamma\,+\right.$$

$$\left.+\int\limits_{\gamma_1}^{\pi/2}\int\limits_0^{\xi'(\gamma)}\frac{\sigma(\xi)\sigma(\xi_1)X(\xi,\gamma)X(\xi_1,\pi-\gamma)}{1+\xi^2\dfrac{H^2}{r^2}\tan^2\dfrac{\gamma}{2}\tan^2\dfrac{\theta_0}{2}}\tan\frac{\gamma}{2}\mathrm{d}\xi\,\mathrm{d}\gamma\right\},$$

where

$$\xi'(\gamma) = \frac{r}{H}\cot\frac{\gamma}{2}; \ \ \gamma_1 \approx \pi - \gamma_2\,.$$

For a homogeneous cloud at $\xi_0 > 1$ the power of the backward scattered signal is

$$P^{(2)}(r) = \frac{P_0 A c \tau_{\mathrm{p}}\sigma_0}{4\pi r^2}e^{-2\tau(r)} \times$$

$$\times\left[\sigma_0(r-H)\int\limits_0^{\gamma_1}X(\gamma)X(\pi-\gamma)\tan\frac{\gamma}{2}\mathrm{d}\gamma\,+\right.$$

$$\left.+\sigma_0 r \tan\frac{\theta_0}{2}\int\limits_{\gamma_1}^{\pi/2}X(\gamma)X(\pi-\gamma)\tan\frac{\gamma}{2}\mathrm{d}\gamma\right].$$

As can be seen from the equation obtained, at $r - H > H\tan\dfrac{\theta_0}{2}$ the double scattered return signal depends both on the depth of pulse propagation into the cloud and on the cross size of the scattering volume at the distance r.

3. Dependence of the double scattered signal intensity on the scattering phase function shape
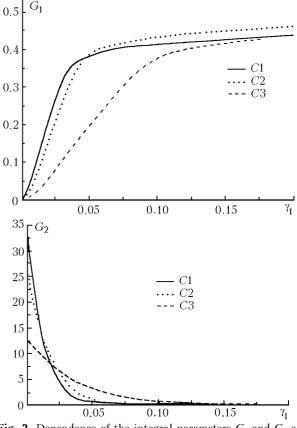
Consider the simplest case: sensing of a homogeneous cloud. The scattering coefficient of such a cloud is independent of the depth and can be described by Eq. (10). In the case of sensing by a

ground-based lidar, the depth of the pulse penetration is larger than the geometrical diameter at the input into the cloud. Let us use Eq. (13), and for a homogeneous plane-stratified cloud we obtain

$$P^{(2)}(r) = \frac{A P_0 c \tau_{\mathrm{p}}\sigma_0}{4\pi r^2}e^{-2\tau(r)}[I_1 + I_2],$$

where

$$I_1 = \sigma_0(r-H)G_1, \quad I_2 = \frac{\sigma_0 r\theta_0}{2}G_2;$$

$$G_1 = \int\limits_0^{\gamma_1}X(\gamma)X(\pi-\gamma)\tan\frac{\gamma}{2}\mathrm{d}\gamma, \quad G_2 = \int\limits_{\gamma_1}^{\pi/2}X(\gamma)X(\pi-\gamma)\mathrm{d}\gamma.$$

Fig. 2. Dependence of the integral parameters G_1 and G_2 on the generalized parameter γ_1 for $C1$, $C2$, and $C3$ cloud models,[10] the wavelength $\lambda = 450$ nm.

The value of $P^{(2)}(r)$ depends on two components I_1 and I_2, which indirectly, through γ_1, depend on the field of view θ_0, the distance to the cloud H, and the sensing depth $(r - H)$. In addition, I_1 significantly depends on the optical thickness of the sensed aerosol, and I_2 increases proportionally to the field of view. At certain values of the lidar field of view and the depth of sensing of an aerosol cloud, I_2 contributes much more to the lidar signal than I_1. As can be seen from Fig. 2, the integral parameters G_1 and G_2 depend on the scattering phase function shape determined by the aerosol microstructure, and they vary most widely in the region of small values of the generalized parameter γ_1.

Thus, the results presented give a methodical basis for separating the lidar signal's portion formed due to double scattering from the total signal. This allows us to plan optimally the experiment, namely, to determine the fields of view of the lidar receiving system, as well as the optical thickness and the sensing depth, at which $P^{(2)}(r)$ is recorded most efficiently, depending on the distance to some aerosol formation.

4. Lidar for measuring a multiply scattered signal

A convenient tool for studying the multiply scattered component in a lidar signal is incoherent spatial filtering of the received radiation in the lidar receiving system.[6,11,12] To investigate experimentally the possibility of such filtering, a specialized lidar was designed at the Institute of Optical Monitoring SB RAS. Its features are a low angular divergence of the sensing radiation and high quality (resolution) of the receiving objective, whose focal plane housed a spatial filter discretely changing the field of view of the receiving system. The filtering permits analyzing the illumination distribution in the image spot of the scattering volume at sensing optically dense aerosol objects, when the received signal includes a multiply scattered component.

The laser transmitter employed the second harmonic of the Nd:YAG laser ($\lambda = 532$ nm). The divergence of the sensing beam was decreased down to 0.8 mrad by an afocal optical system with the magnification $\Gamma = 10^{\times}$. Lenses with corrected spherical aberration were used as optical antennae in the transmitting and receiving systems. At the relative aperture of the receiving objective 1:5 and the focal length of the lens $f = 750$ mm, the diameter of the point image spot did not exceed 24 μm in the linear field of view with the diameter up to 16 mm. To improve the image in the near zone without significant loss in quality in the far zone and at infinity, we used a hyperfocal installation of the receiving objective relative to the plane of windows of the spatial filter $f + (0.3–0.5)$ mm.

We replaced the initially accepted coaxial arrangement of the transceiver by the biaxial one, which ensured a higher rigidity of the construction and stability of alignment of the optical axes of the transmitter and the receiving system (no more than 0.1 mrad). At the same time, this decreased the energy loss and diffraction distortions of the signal at the input aperture. At the basic distance between the axes of the transmitter and the receiving system equal to 144 mm, the effect of parallax almost does not show itself starting from the distances $z = 150–200$ m, that is, almost immediately beyond the limits of marked manifestation of the near-zone defocusing of the receiving system. A FEU-84-3 photomultiplier tube operating in the current mode was used as a photodetector in the lidar. The frequency band of the photodetector output circuit was 20 MHz.

We used the simplest, in design, spatial filter of the integrating type: a round window with the discretely changing radius R_o (Fig. 3a). Other shapes of the window are possible as well,[13] for example, when the ring radius R_k is varied discretely at the constant ring width ΔR or when the radius of an occluding circle R_{occl} is varied at the constant window radius R_{max} (the differentiating and matched filters, Figs. 3b, c).

The functional layout of the lidar is shown in Fig. 4. The filter is made as a turret disk 7, which is rotated by an electric motor 13 with the rate of 3 rev/s, successively setting into the working position with the frequency of 24 Hz the round windows of 1, 2, 3, 4, 6, 8, 10, and 12 mm in diameter. The transmitter operation is synchronized by a photon-coupled pair 14, 15 and a series of specialized holes on the disk edge. To synchronize the process of grouping the digitized signals by the window size, the system includes an additional photon-coupled pair 14, 16 connected to a computer. It synchronizes the operation of signal recording devices with the beginning of every new window changing sequence (the time of placing the window of the minimal size into the working position). Signals are digitized and recorded by a 7-bit ADC; the digitizing frequency is 20 MHz.

The fast and continuous window changing, grouping the ensembles of digitized signals corresponding to each of filter windows, and then calculating the family of averaged signals permit decreasing the contribution of dynamic variations of sensed objects to the result of lidar measurements.
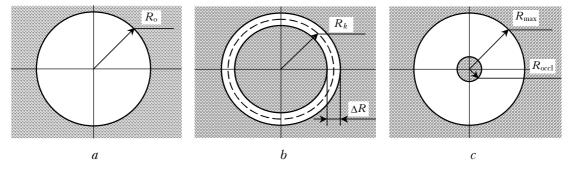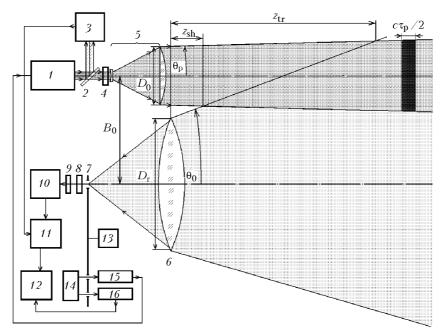

Fig. 3. Windows of spatial filters: integrating filter (*a*), differentiating filter (*b*), and matched filter (*c*).

Fig. 4. Lidar functional layout: laser *1*; glass beam-splitting plate *2*; sensor for starting ADC and processing devices *3*; polarization filter *4*; collimator *5*; receiving objective *6*; disk with spatial filtering windows *7*; polarization filter *8*; spectral filter *9*; photodetector *10*; ADC *11*; IBM PC *12*; electric motor *13*; sensor transmitters *14*; sensor for starting the laser *15*; sensor for starting the data grouping process *16*.

Each family obtained consists of eight averaged lidar signals (corresponding to the number of filter windows). The number of window changing sequences (number of signal realizations in each ensemble) and the recording range (number of readouts in the range) are preset before the beginning of every lidar measurement.

The image spot of the scattering volume projected in the focal plane of the receiving system of the lidar has an axial (central) symmetry starting already from the distance $z > 200$ m. The illumination (lidar signal power density) distribution in the image plane can be described by the function $b(z, \rho)$, where ρ is the distance from the spot geometrical center (from the axis of the receiving system). The actual form of the function $b(z, \rho)$ depends on the transceiver parameters and the sensed medium characteristics. The power of the radiation flux coming from the distance z and bounded by a round diaphragm of the radius R in the image plane is

$$P(z, R) = 2\pi \int_0^R b(z, \rho)\rho d\rho. \qquad (14)$$

The power of the averaged signals at every point of the range z_j can be found by averaging the signal realizations at this point for ensembles corresponding to each of eight values of the radius R_k of the filter window ($k = 1, 2, ..., 8$). Thus, we analyze some averaged distributions in ensembles (by the number of window changing sequences).

In the experimental investigations,[14] it was proposed to use the Gauss function to describe the spatial distribution of the power density of the lidar

return signal caused by MS in artificial fogs and smokes at their irradiation by continuous-wave laser radiation. This suggests that

$$b(z, \rho) = b(z)\exp\{-[\rho/a(z)]^2\}. \qquad (15)$$

Such an approach allows us to reduce the further analysis of lidar signals to determination of the normal distribution parameters: the energy parameter $b(z)$ — the power density at the center of the analyzed spot and the spatial parameter $a(z)$ — the size of this spot. The values of these parameters are connected with the properties of the medium under sensing. Their dependences on the range z reflect, in the best way, the dynamics of variation of the scattering volume, i.e., the return signal source. Substituting Eq. (15) into Eq. (14), for every signal in the each ith window changing sequence we can obtain the power P_{ijk} recorded at every point of the range z_j for each window k (in each ensemble):

$$P_{ijk} = P_i\big(z_j, R_k\big) =$$
$$= \pi a^2(z_j)\,b(z_j)\{1 - \exp[-(R_k/a(z_j))^2]\}_i. \qquad (16)$$

Based on the ensemble of the experimentally obtained P_{ijk} values, we calculate the family of the averaged signals $\overline{P_{jk}} = \sum_{i=1}^{n} P_{ijk}$, for the preset value n of the window changing sequences; the family of S-functions $S_{jk} = \overline{P_{jk}}z_j^2$; the family of the log$S$-functions $\ln S_{jk} = \ln \overline{P_{jk}}\,z_j^2$ for the use in subsequent applications. Parameters $a(z)$ and $b(z)$ of the distribution (15) are connected with the scattering

phase function and microphysical characteristics of scattering particles on the path. And the stronger is the inequality $(D_0 + 2\theta_p z)/2 < A(z)$, where D_0 is the beam diameter at the transmitter exit and $A(z)$ is the effective radius of the scattering volume at the distance z (in the object space), the weaker is the effect of the sensing beam characteristics.

To determine the parameters of the power density distribution, Eq. (16) is reduced to the form

$$P_k = B[1 - \exp(-CR_k^2)], \qquad (17)$$

where

$$C = 1/a^2; \ B = \pi a^2 b.$$

Equation (17) has independent solutions at every point of the range, since parameters a and b are functions of the distance z_j. They are determined by the least-square method. The value

$$B_0 = \frac{\sum\limits_k P_k \left[1 - \exp\left(-C_0 R_k^2\right)\right]}{\sum\limits_k \left[1 - \exp\left(-C_0 R_k^2\right)\right]^2}. \qquad (18)$$
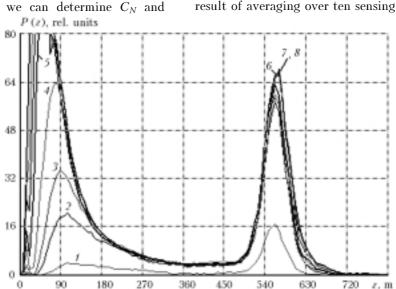
best fits the preset value C_0, and the correction

$$\Delta C_1 = \frac{\sum P_k R_k^2 \exp(-C_0 R_k^2)}{\sum\limits_k B_0 R_k^4 \exp\left(-2C_0 R_k^2\right)} -$$

$$- \frac{\sum B_0 R_k^2 \exp(-C_0 R_k^2)[1 - \exp(-C_0 R_k^2)]}{\sum\limits_k B_0 R_k^4 \exp\left(-2C_0 R_k^2\right)}. \qquad (19)$$

best fit the values C_0 and B_0. The correction ΔC_1 refines the solution. In this case, every new, refined value C_1 is determined as

$$C_1 = C_0 + \Delta C_1. \qquad (20)$$

Repeating the procedures (18)–(20), we can find new values B_1, ΔC_2 and C_2 and refine the solution of Eq. (17). Repeating the iteration procedures many times, we can determine C_N and

B_N, where N is the number of iterations, at which $\Delta C_N / C_N \le \delta$ (here δ is the preset relative error of calculation).

The final results of such calculation are the distribution parameters of the lidar signal power density in the plane of the spatial filter for every point of the range z_j

$$a(z) = \frac{1}{\sqrt{C_N(z)}} \ \text{and} \ b(z) = \frac{C_N(z) B_N(z)}{\pi}.$$

Based on these values, we can determine the asymptotic signal, the power of the lidar return, under the condition that the radius of the filter window $R_k \gg a(z)$ in Eq. (16)

$$P(z)\big|_{R\ \ a} = \pi a^2(z) b(z) \qquad (21)$$

and the parameters of the energy brightness distribution in the lidar plane of observation (object plane) are

$$A(z) = \frac{a(z) z}{f} \ \text{and} \ B(z) = \frac{4 b(z)}{\pi q^2},$$

where $q = D_r/f$ is the relative aperture of the receiving objective, and D_r is the diameter of its input aperture. The asymptotic signal (21) can be also determined through the parameters $A(z)$ and $B(z)$ of the scattering volume

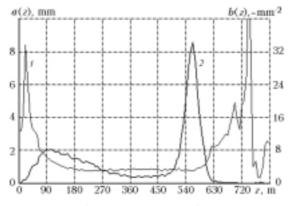$$P(z)\big|_{R\ \ a} = \frac{\pi^2 [A(z)]^2 B(z) D^2}{4 z^2}.$$

5. Experimental results

Figure 5 depicts a family of eight lidar returns (corresponding to the number of filter windows with different sizes $2R_k$) obtained from sensing a cloud spaced by 470 m from the lidar. Each signal is the result of averaging over ten sensing cycles.

Fig. 5. Family of averaged lidar signals at different sizes of the filter windows: $2R = 1$ (*1*), 2 (*2*), 3 (*3*), 4 (*4*), 6 (*5*), 8 (*6*), 10 (*7*), and 12 mm (*8*).

Thus, the presented eight curves are obtained based on 80 sensing events made with the repetition frequency of 24 Hz for the interval of 3.33 s. The difference in the signal amplitude at the initial part of the path is caused by the different sizes of the shadow z_{sh} and transient z_{tr} reception zones for each window (see Fig. 4).

The largest size of the shadow and transient zones corresponds to the smallest window. As the size of the filter window increases, the power of the recorded signals increases in both the lidar transient zone (the first 180 m) and nearby the cloud. The latter is indicative of the presence of multiple scattering. The difference in the signal amplitude is especially marked at the end of the sensing path, where the energy contribution of multiple scattering prevails. Absolutely all signals in the obtained families correlate well with each other beyond the transient zone, which is indicative of insignificant manifestation of dynamic variations of the sensed object in the interval of 3.33 s. Technically, most difficult is realization of lidar measurements with the smallest windows. In the cases that the field of view of the receiving system is close to the angular divergence of the transmitter radiation ($\theta_0 \approx \theta_p$), even minor misalignments of the optical axes of the transmitter and the receiving system become considerable. In our case, the level of the signal *1* at the range of 270−500 m is limited by manifestation of such misalignment.

Based on the family of the averaged signals, we have calculated the distribution parameters of the lidar signal power density in the plane of the spatial filter. The calculated results are depicted in Fig. 6.

Fig. 6. Calculated parameters of a lidar signal: variation of the cross size of the image spot $a(z)$ (*1*) and power density $b(z)$ at the center of this spot (*2*).

The energy parameter $b(z)$, which is, physically, the power density of the lidar signal at the spot center, qualitatively copies the dynamics of signal variation in the initial family (see Fig. 5). The spatial parameter $a(z)$, being the effective spot radius, within the transient zone is caused by manifestation of parallax; beyond the near zone and up to the cloud it varies insignificantly. Under single scattering conditions, $a(z)$ is determined by the

angular size of the transmitted beam cross section. The following growth of $a(z)$ is connected with the increase of the observed angular size of the scattering volume, which is caused by the repeated scattering events in the cloud.

Using $a(z)$ and $b(z)$, we can separate the lidar signal $P(z)$ into the single and multiply scattered components $P^{(1)}(z)$ and $P^{(2)}(z)$. The power of $P^{(1)}(z)$ is concentrated in the central zone of the image, and its value can be estimated as
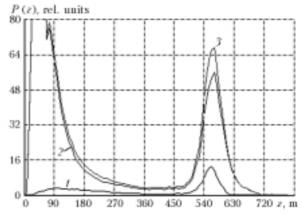
$$P^{(1)}(z) = \pi(\bar{a})^2 b(z),$$

where $\bar{a}$ is the effective radius of the image of the transmitted beam cross section, which determines the cross size of the single scattering volume. The multiply scattered component can be estimated as

$$P^{(2)}(z) = P(z) - P^{(1)}(z).$$

As the initial (total) signal $P(z)$, we used $P_8(z)$ from the family of averaged signals, which almost coincides with the asymptotic signal (21). The radius $\bar{a}$ of the image spot can be estimated by averaging $a(z)$ on the range part, where $a(z) \approx$ const. However, this estimate may include an error, if the signals on the averaging interval include the multiply scattered component. We estimated the radius $\bar{a}$ based on the analysis of the family of signals received in the case of sensing a scattering screen. The estimated $\bar{a}$ is equal to the spatial parameter $a(z_{scr})$ at the distance z_{scr} equal to the distance to the screen. Its value beyond the transient zone, 0.35 mm, is independent of the range, and was used as a calibration constant.

Figure 7 depicts the total signal $P_8(z)$ and its components $P^{(1)}(z)$ and $P^{(2)}(z)$ estimated as described above. As can be seen from Fig. 7, beyond the transient zone and up to the cloud, the single scattered signal *1* almost copies the signal *1* in the initial family corresponding to the smallest window (see Fig. 4), in which MS is low. And the MS signal *2* is close to the total signal *3*. Deeper in the cloud, the energy contribution of MS to the total signal becomes predominant, as in the transient zone ($z < 180$ m).

Fig. 7. Separation of the components of the lidar return signal $P(z)$: $P^{(1)}(z)$ (*1*), $P^{(2)}(z)$ (*2*), total signal (*3*).

The quality of the presented estimates can be quite sufficient for practical applications.

Acknowledgments

References

1. I.N. Polonskii, E.P. Zege, and I.L. Katsev, Izv. Ros. Akad. Nauk, Fiz. Atmos. Okeana **37**, No. 5, 672–680 (2001).

2. P. Bruscalioni, A. Ismaelli, and G. Zaccanti, Appl. Phys. B **60**, 325–329 (1995).

3. L.R. Bissonnette and D.L. Hutt, Appl. Opt. **34**, No. 30, 6959–6975 (1995).

4. E.W. Eloranta, Appl. Opt. **40**, 2464–2472 (1998).

5. V.V. Veretennikov, A.I. Abramotchkin, and S.A. Abramotchkin, Proc. SPIE **5059**, 179–188 (2002).

6. I.A. Razenkov, I.V. Samokhvalov, and S.N. Targonskii, Opt. Atm. **1**, No. 12, 22–25 (1988).

7. V.E. Zuev, B.V. Kaul', I.V. Samokhvalov, K.I. Kirkov, and V.I. Tsanev, *Laser Sensing of Industrial Aerosols* (Nauka, Novosibirsk, 1986), 188 pp.

8. I.V. Samokhvalov, Izv. Akad. Nauk SSSR, Fiz. Atmos. Okeana **XV**, No. 12, 1271–1279 (1979).

9. I.V. Samokhvalov and V.V. Bryukhanova, in: *Proc. of Second Baikal School on Fundamental Physics* (Irkutsk, 1999), pp. 444–449.

10. D. Deirmendjian, *Electromagnetic Scattering on Spherical Polydispersions* (American Elsevier, New York, 1969).

11. A.I. Abramochkin and A.A. Tikhomirov, Atmos. Oceanic Opt. **12**, No. 4, 331–342 (1999).

12. A.A. Tikhomirov, Izv. Vyssh. Uchebn. Zaved., Fiz., No. 10, 93–104 (2001).

13. A.I. Abramochkin, S.A. Abramochkin, and A.A. Tikhomirov, Proc. SPIE **3983**, 458–462 (1999).

14. V.A. Donchenko, I.V. Samokhvalov, and G.G. Matvienko, Izv. Akad. Nauk SSSR, Fiz. Atmos. Okeana **VII**, No. 11, 1183–1189 (1971).